DISCRETE AND CONTINUOUS
DYNAMICAL SYSTEMS
Volume **4**, Number **4**, October **1998** pp. **609–634**

ON TWO-DIMENSIONAL RIEMANN PROBLEM FOR PRESSURE-GRADIENT EQUATIONS OF THE EULER SYSTEM

Peng Zhang

Beijing Information and Technology Institute, Beijing, 100101

Jiequan Li

Institute of Applied Mathematics, Academia Sinica, Beijing, 100080

Tong Zhang

Institute of Mathematics, Academia Sinica, Beijing, 100080

(Communicated by Fanghua Lin)

Abstract. We consider the two-dimensional Riemann problem for the pressure-gradient equations with four pieces of initial data, so restricted that only one elementary wave appears at each interface. This model comes from the flux-splitting of the compressible Euler system. Lack of the velocity in the eigenvalues, the slip lines have little influence on the structures of solutions. The flow exhibits the simpler patterns than in the Euler system, which makes it possible to clarify the interaction of waves in two dimensions. The present paper is devoted to analyzing the structures of solutions and presenting numerical results to the two-dimensional Riemann problem. Especially, we give the criterion of transition from the regular reflection to the Mach reflection in the interaction of shocks.

1. Introduction. We are concerned with the pressure-gradient equations of the compressible Euler system

$$\begin{cases} \rho_t = 0, \\ (\rho U)_t + \nabla p = 0, \\ (\rho E)_t + \nabla \cdot (pU) = 0, \end{cases} \tag{1.1}$$

where $\rho(t, X) \geq 0$ ($X = (x, y)$) is the density, $U = (u, v)$ is the velocity, $p \geq 0$ is the pressure, $E = e + |U|^2/2$ denotes the total energy per unit mass, e denotes the internal energy given by $e = p((\gamma-1)\rho)^{-1}$ for polytripic gases, $\gamma > 1$ is the adiabatic index, ∇ designates the gradient operator with the space variable X. This system comes from the flux-splitting method in numerical analysis on the Euler system

$$\begin{cases} \rho_t + \nabla \cdot (\rho U) = 0, \\ (\rho U)_t + \nabla \cdot (\rho U \otimes U) + \nabla p = 0, \\ (\rho E)_t + \nabla \cdot (pU(E + \dfrac{p}{\rho}) = 0, \end{cases} \tag{1.2}$$

by separating the pressure from the inertia in the flux [AH, LC]. The pressure-gradient equations (1.1) are valid whenever the inertia effect is so small compared to the pressure-gradient effect of the flow as to be negligible. As a matter of fact, assuming that the velocity U is small, we can obtain ρ_t from the first equation of

1991 *Mathematics Subject Classification.* 35L65, 58F40, 65M06, 76N10.

Key words and phrases. pressure-gradient equations, two-dimensional Riemann problem, rarefaction wave, shock, slip line, regular reflection, Mach reflection, MmB scheme.

The second author was supported by State Key Laboratory of Scientific and engineering computing, Academia Sinica. The third author was supported by National Fundamental Research Program of State Commission of Scien. and Tech. of China, and Academia Sinica.

(1.2), and then the second equation can be derived from the conservation law of momentum of (1.2) because the quadratic terms $\nabla\cdot(\rho U\otimes U)$ are much smaller than the linear terms $(\rho U)_t$ or the pressure-gradient terms ∇p which are supposed to be large, while the last equation can be found after dropping the cubic terms from the energy equation of (1.2) due to the similar reasons. Thus, the pressure-gradient equations (1.1) have their own physical value.

The eigenvalues of this system in the direction (μ,ν) with $\mu^2+\nu^2=1$ are

$$\lambda_0=0,\qquad \lambda_\pm=\pm\sqrt{\frac{\gamma-1}{\gamma}}c, \tag{1.3}$$

where $c=\sqrt{\gamma p\rho^{-1}}$ is the sonic speed. These eigenvalues are independent of the velocity U, compared with those of the Euler system. We also point out that the vorticity of the flow is unchanged as the time passes. Therefore, this flow exhibits more simplicity.

Noting that the density ρ remains unchanged as time increases, we hope to simplify (1.1) slightly but not to change the essential nonlinear structure of the flow. We always assume, from now on, that

$$\rho\equiv 1$$

instead of $\rho_t=0$, and further take the transformation $(\gamma-1)^{-1}p\to p'$ and $(\gamma-1)^{-1}X\to X'$. Then (1.1) can be reduced to the system

$$\begin{cases} U_t+\nabla p=0,\\ E_t+\nabla\cdot(pU)=0, \end{cases} \tag{1.4}$$

where $E=p+\dfrac{|U|^2}{2}$, and primes on X' and p' are dropped just for simplicity. For a smooth solution or in the region where the solution is smooth, (1.4) can be written as

$$\begin{cases} U_t+\nabla p=0,\\ p_t+p\nabla\cdot U=0. \end{cases} \tag{1.5}$$

Therefore, we can obtain the wave equation

$$(\frac{p_t}{p})_t=\triangle p, \tag{1.6}$$

where $\triangle=\partial_{xx}+\partial_{yy}$ is the Laplace operator. This is very interesting and may be one of the simplest second order quasi-linear hyperbolic equations awaiting for the investigation. In the self-similar plane, (ξ,η)-plane ($(\xi,\eta)=(x/t,y/t)$), (1.6) or (1.4) is of mixed-type. Throughout the present paper we just pay our attention to (1.4) rather than the original one (1.1).

In this paper, we consider the Riemann problem for (1.4). The initial data is constant in each quadrant,

$$(p,u,v)(0,x,y)=(p_i,u_i,v_i),\quad i=1,2,3,4, \tag{1.7}$$

which is so restricted that only one elementary wave, a rarefaction wave, a shock, or a slip line appears at each interface. We follow the same steps as in [ZZ] to analyze the structure of solutions and present the numerical results with MmB scheme (local maximum and minimun bounds preserving), which is applicable to a wide variety of applications [WS]. This problem is discussed in the self-similar plane according to the different combinations of elementary waves at the interface of initial data. We classify twelve genuinely different configurations for the system (1.4). Each of them is analyzed with the method of characteristics, the boundaries of interaction domains are clarified, and the corresponding numerical result is illustrated by the contour plots of pressure and self-similar Mach number. A lot of problems never

considered before are proposed. We explicitly give the criterion of transition from the regular reflection to the Mach reflection in the interaction of shocks. By the comparision with the conjecture in [ZZ], we find that this system is very useful to understand the complicated flow patterns of the Euler system.

In Section 2, We discuss the resulting self-similar equations of (1.4) and classify the combinations of elementary waves. We analyze the structure of solutions and present the numerical solutions in Section 3, which contains the description of wave interaction. Our discussions are given in Section 4.

2. Characteristics, discontinuities, elementary waves and classifications. In this section we present a preliminary analysis on (1.4) and give the classification of combinations of the elementary waves at each interface of initial data.

2.1 Characteristics. For smooth solutions, (1.4) can be reduced to the self-similar form

$$\begin{cases} -\xi u_\xi - \eta u_\eta + p_\xi = 0, \\ -\xi v_\xi - \eta v_\eta + p_\eta = 0, \\ -\xi E_\xi - \eta E_\eta + (pu)_\xi + (pv)_\eta = 0. \end{cases} \tag{2.1}$$

This system can be simplified into a second order partial differential equation after u and v have been eliminated

$$(p-\xi^2)p_{\xi\xi} - 2\xi\eta p_{\xi\eta} + (p-\eta^2)p_{\eta\eta} + \frac{1}{p}(\xi p_\xi + \eta p_\eta)^2 - 2(\xi p_\xi + \eta p_\eta) = 0, \tag{2.2}$$

which can also be derived from (1.6) by the same coordinate transformation and is named the transonic pressure-gradient equation of Euler system.

The initial data (1.7) becomes

$$\lim_{\xi^2+\eta^2\to\infty}(u,v,p) = (u_i, v_i, p_i), \quad (\xi,\eta) \text{ in the } i^{th} \text{ quadrant.} \tag{2.3}$$

The eigenvalues of (2.1) or (2.2) are

$$\lambda_0 = \frac{\eta}{\xi}, \qquad \lambda_\pm = \frac{\xi\eta \pm \sqrt{p(\xi^2+\eta^2-p)}}{\xi^2 - p}. \tag{2.4}$$

λ_0 is obviously linear, while $\lambda_\pm$ may be real or complex depending on whether or not $\xi^2+\eta^2 > p$.

Define characteristic curves Γ_j $(j = 0, \pm)$ in the (ξ,η)-plane by

$$\Gamma_j : \quad \frac{d\eta}{d\xi} = \lambda_j,$$

which are called pseudo-characteristics (characteristics for abbreviation) of (1.4) in the supersonic domain for a given solution $(u,v,p)(\xi,\eta)$. Each of these characteristic curves has an end-point, which results from the geometry singularity of initial data at the origin. Obviously, on the sonic circle $\xi^2+\eta^2 = c^2$ $(c^2 = p)$, $\Gamma_\pm$ are tangent to the sonic circle and perpendicular to Γ_0. We orient each characteristic from the infinity to its end-point.

Call that the vectors n_1 and n_2 form a left-hand system if the angle from n_1 to n_2 is less than π and greater than zero; otherwise, the vectors n_1 and n_2 form a right-hand system, as shown in Figure 2.1. Then we can give the following definition.

Right-hand system

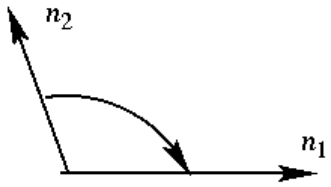

Left-hand system

Figure 2.1

Definition 1.1 *A smooth solution is called a rarefaction wave, denoted by R, if the pressure decreases along a slip line. The rarefaction wave can be classified into two kinds, $R^{\pm}$:*

$R = R^+$ if $\nabla_{\xi\eta} p$ and the direction of slip line form a left-hand system;

$R = R^-$ if $\nabla_{\xi\eta} p$ and the direction of slip line form a right-hand system.

2.2 Discontinuity. Let $\eta = \eta(\xi)$ be a smooth discontinuity of a bounded discontinuous solution of (1.4) or (2.1) with the normal $(\xi\sigma - \eta, -\sigma, 1)$ $(\sigma = \dfrac{d\eta}{d\xi})$. Then the Rankine-Hugoniot relation should hold, i.e.,

$$\begin{cases} (\xi\sigma - \eta)[u] - \sigma[p] = 0, \\ (\xi\sigma - \eta)[v] + [p] = 0, \\ (\xi\sigma - \eta)[E] - \sigma[pu] + [pv] = 0, \end{cases} \tag{2.5}$$

where the quantity in the bracket is the jump across the discontinuity. We can find by solving these either a linear discontinuity

$$\begin{cases} \sigma_0 = \dfrac{\eta}{\xi} = \dfrac{[v]}{[u]}, \\ [p] = 0, \end{cases} \tag{2.6}$$

or nonlinear discontinuities

$$\begin{cases} \dfrac{d\eta}{d\xi} = \sigma_{\pm} = -\dfrac{[u]}{[v]} = \dfrac{\xi\eta \pm \sqrt{\overline{p}(\xi^2 + \eta^2 - \overline{p})}}{\xi^2 - \overline{p}}, \\ [p]^2 = \overline{p}([u]^2 + [v]^2), \end{cases} \tag{2.7}$$

where $\overline{p} = \dfrac{p + p_1}{2}$ is the average of the pressures on the two sides of the discontinuity. Compared with (2.4), the nonlinear discontinuities (2.7) can never be tangent to the flow line or the $\lambda_{\pm}$ characteristic lines. We can also conclude that

$$\begin{cases} [p] = \xi[u] + \eta[v], \\ [u] = \dfrac{\xi\overline{p} \pm \eta\sqrt{\overline{p}(\xi^2 + \eta^2 - \overline{p})}}{\overline{p}(\xi^2 + \eta^2)}[p], \\ [v] = \dfrac{\eta\overline{p} \mp \xi\sqrt{\overline{p}(\xi^2 + \eta^2 - \overline{p})}}{\overline{p}(\xi^2 + \eta^2)}[p] \end{cases} \tag{2.8}$$

corresponding to $\sigma_{\pm}$ respectively. This system has only two independent equations, but it gives an accurate relation between the states on the wave front and wave back of shocks. It is expected to be useful in solving the boundary value problem for (2.1) with a shock as the boundary.

Denote $\overline{c}^2 = \overline{p}$, and call $\xi^2 + \eta^2 = \overline{c}^2$ a Rankine-Hugoniot circle (R-H circle for short) similar to the sonic circle $\xi^2 + \eta^2 = c^2$. Therefore an R-H circle must be

located between two sonic circles $C_1 : \xi^2 + \eta^2 = c^2$ and $C_2 : \xi^2 + \eta^2 = c_1^2$ unless either p or p_1 vanishes. Just like the characteristics, a nonlinear discontinuity (2.7) is tangential to the corresponding R-H circle and perpendicular to a linear discontinuity there, and it has a tangent point on R-H circle as its end-point, due to the geometry singularity of initial data at the origin. We also orient the discontinuity (2.6) from infinity to the origin and (2.7) from infinity to its end-point respectively.

Definition 2.2 *A discontinuity is called a contact discontinuity or a slip line, denoted by J, if it satisfies (2.6). A slip line can be classified into two kinds according to the sign of vorticity, that is*

$$J^{\pm} : curl(u, v) = \pm\infty. \tag{2.9}$$

A discontinuity is called a shock, denoted by S, if it satisfies (2.7) and the pressure p increases across it along a slip line, that is, the pressure on the wave front is larger than on the wave back. The shock can be classified into two kinds:

$S = S^+$ if $\nabla_{\xi\eta} p$ and the direction of slip line form a right-hand system;

$S = S^-$ if $\nabla_{\xi\eta} p$ and the direction of slip line form a left-hand system.

2.3 Planar elementary waves. Consider bounded solutions of the form $(u, v, p)(\xi)$ or $(u, v, p)(\eta)$. We call these planar elementary waves (exterior waves). We discuss the following four cases as examples; the other cases can be treated similarly. Here we denote (u_1, v_1, p_1) and (u_2, v_2, p_2) the states on the wave front and the wave back.

(i) Constant states: $(u, v, p) = (u_0, v_0, p_0) = const.$

(ii) Rarefaction waves:

$$R^{\pm}(\xi) : \begin{cases} \xi = \sqrt{p}, \quad p_2 < p_1, \\ [u] = 2[\sqrt{p}], \\ [v] = 0, \\ \eta \overset{>}{<} 0. \end{cases} \tag{2.10}$$

(iii) Shock waves:

$$S^{\pm}(\xi) : \begin{cases} \xi = \sqrt{\overline{p}}, \quad p_2 > p_1, \\ [u] = \dfrac{[p]}{\sqrt{\overline{p}}}, \\ [v] = 0, \\ \eta \overset{>}{<} 0. \end{cases} \tag{2.11}$$

(iv) Slip lines

$$J^{\pm} : \begin{cases} \xi = \sigma_0 = 0, \\ [p] = 0, \\ [u] = 0, \\ curl(u, v)|_J = \pm\infty. \end{cases} \tag{2.12}$$

The last expression in (2.12) is also equivalent to $v_2 < v_1$ or $v_2 > v_1$ corresponding to the signs "minus" or "plus".

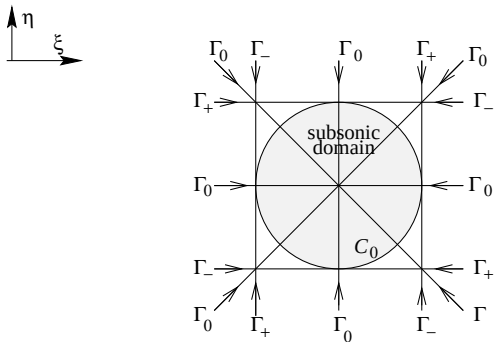

Figure 2.2

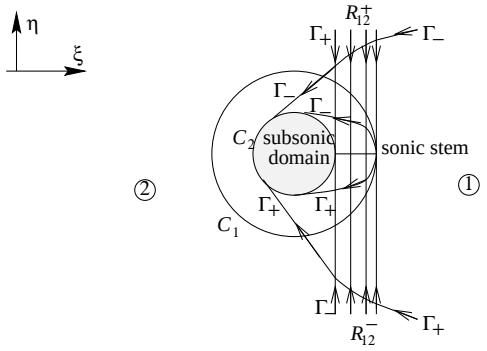

Figure 2.3

We can analyse the following facts about planar elementary waves with the same method as in [ZZ].

(i) The solution is a constant state $(u, v, p) = (u_0, v_0, p_0)$. Its sonic curve is the circle

$$C_0: \quad \xi^2 + \eta^2 = p_0.$$

This flow is subsonic inside the circle and supersonic outside the circle. The slip line is a ray through the origin. Each of the characteristics $\Gamma_\pm$ is a ray from infinity to the sonic circle tangentially. The clockwise ray corresponds to Γ_- and the counterclockwise ray corresponds to Γ_+, as illustrated in Figure 2.1.

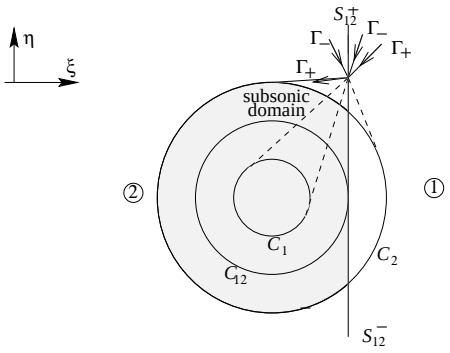

Figure 2.4

(ii) $R_{12}^+(\xi)$ $(\eta > 0)$ and $R_{12}^-(\xi)$ $(\eta < 0)$ connecting two constant states (u_2, v_2, p_2) and (u_1, v_1, p_1), as drawn in Figure 2.2. Γ_0 are half-ray lines with the origin as the vertex. $\Gamma_\pm$ are

$$\Gamma_+ : \begin{cases} \xi = \sqrt{p}, & \text{if } \eta > 0, \\ (\xi - k)^2 + \eta^2 = k^2, & \text{if } \eta < 0, \end{cases} \qquad \Gamma_- : \begin{cases} (\xi - k)^2 + \eta^2 = k^2, & \text{if } \eta > 0, \\ \xi = \sqrt{p}, & \text{if } \eta < 0. \end{cases}$$

where $k > c_2$ is an arbitrary constant.

The sonic curve of $R_{12}^+(\xi)$ $(\eta > 0)$ and $R_{12}^-(\xi)$ $(\eta < 0)$ is

$$\eta = 0, \qquad (\sqrt{p_2} \le \xi \le \sqrt{p_1}),$$

which is called the sonic stem.

(iii) $S_{21}^+(\xi)$ $(\eta > 0)$ and $S_{21}^-(\xi)$ $(\eta < 0)$ connecting two constant states (u_2, v_2, p_2) and (u_1, v_1, p_1), as drawn in Fig.2.3. $S_{21}^{\pm}(\xi)$ is tangent to the R-H circle

$$C_{12}: \quad \xi^2 + \eta^2 = \frac{p_1 + p_2}{2}.$$

Since $c_1 < \sigma_{12} < c_2$, the sonic circle C_1 and the part of the sonic circle C_2 are imaginary. And on two sides of a point on $S_{21}^{\pm}(\xi)$ in the supersonic domain, there are three nonlinear characteristic lines are incoming while the left is outgoing, as shown in Figure 2.3.

(iv) $J_{21}^{\pm}$ connecting two constant states (u_2, v_2, p_2) and (u_1, v_1, p_1).

$$J_{21}^{\pm}: \begin{cases} \xi = 0, \\ p_1 = p_2, \\ u_1 = u_2, \end{cases} \tag{2.13}$$

where the sign "plus" or "minus" is equivalent to that $v_2 < v_1$ or $v_2 > v_1$. Since the pressures on two sides are equal, the sonic circles C_1 and C_2 are the same and the halves are imaginary. The two constant states are cut off to shift with different velocities.

2.4 Classification. Under the restriction that the initial data (2.1) is so chosen that only a shock wave, a rarefaction wave or a contact discontinuity appears at each interface, there exist 12 genuinely different combinations of exterior waves except three trivial cases, since all other combinations can be transformed into these cases by coordinate rotation and/or reflection transformations.

$4R:$	$R_{12}^+R_{23}^+R_{34}^-R_{41}^-,$	$R_{12}^+R_{23}^-R_{34}^+R_{41}^-;$	
$4S:$	$S_{12}^-S_{23}^+S_{34}^-S_{14}^+,$	$S_{12}^-S_{23}^-S_{34}^+S_{41}^+;$	
$2R+2S:$	$S_{12}^-R_{23}^-S_{34}^-R_{14}^-;$		
$2J+2R:$	$R_{12}^+J_{23}^+J_{34}^-R_{14}^-,$	$R_{12}^-J_{23}^+J_{34}^-R_{14}^+;$	
$2J+2S:$	$S_{12}^-J_{23}^-J_{34}^+S_{14}^+,$	$S_{12}^+J_{23}^-J_{34}^+S_{14}^-;$	
$2J+R+S:$	$R_{12}^+J_{23}^+J_{34}^+S_{14}^+,$	$R_{12}^-J_{23}^+J_{34}^+S_{14}^-,$	$J_{12}R_{23}^-J_{34}S_{14}^-.$

3. The analysis on the structures of solutions and numerical results. In this section, we will analyze the structure of solutions to the Riemann problem with the generalized characteristic method, and then present the numerical solutions. The following abbreviations are often used,

$$\Phi_{ij} = 2(\sqrt{p_i} - \sqrt{p_j}), \quad \Psi_{ij} = \frac{p_i - p_j}{\sqrt{\dfrac{p_i + p_j}{2}}}, \tag{3.1}$$

where $ij \in \{12, 23, 34, 41\}$. These abbreviations satisfy

$$\Phi_{ij} = -\Phi_{ji}, \qquad \Psi_{ij} = -\Psi_{ji}. \tag{3.2}$$

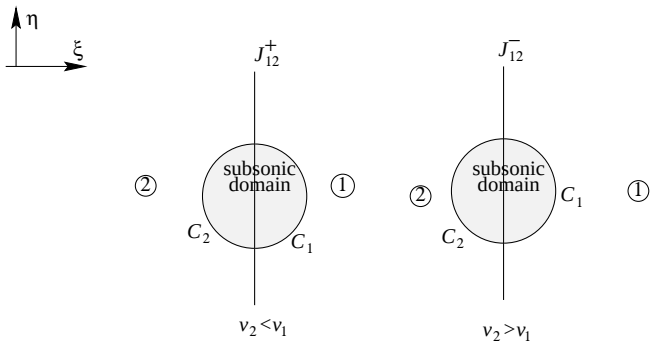

Figure 2.5

3.1 The interaction of four rarefaction waves. There are two cases for the interaction of four rarefaction waves and each of them has two subcases.

Configuration A $R_{12}^+R_{23}^+R_{34}^-R_{14}^-$.

The four constant states must satisfy the following system (A):

$$\begin{aligned} R_{12}^+ &: \quad u_1-u_2=\Phi_{12}, \quad v_1=v_2, \quad p_1>p_2,\\ R_{23}^+ &: \quad v_2-v_3=\Phi_{23}, \quad u_2=u_3, \quad p_2>p_3,\\ R_{34}^- &: \quad u_4-u_3=\Phi_{43}, \quad v_4=v_3, \quad p_4>p_3,\\ R_{41}^- &: \quad v_4-v_1=\Phi_{41}, \quad u_1=u_4, \quad p_1>p_4. \end{aligned} \tag{3.3}$$

Therefore, $\sqrt{p_1}+\sqrt{p_3}=\sqrt{p_2}+\sqrt{p_4}$. For any fixed p_1, u_1, v_1, p_2, p_3, we can obtain p_4, u_i, v_i $(i=2,3,4)$ from the first column and the second column of (3.3).

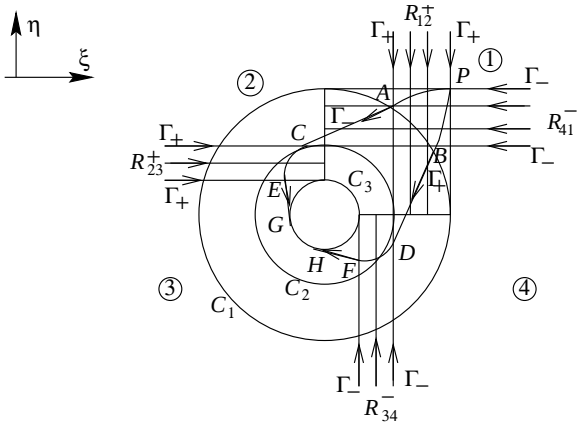

Figure 3.1

$R_{12}^+(\xi)$ and $R_{14}^-(\eta)$ from the infinity meet together at P before they reach their own sonic circles. Then they will interact with each other. So, the part of the boundary of the interaction region should be extension of characteristic lines Γ_- and Γ_+ from P. Γ_- penetrates $R_{12}^+(\xi)$ and ends at A firstly and then goes straight until it intersects $R_{23}^-(\eta)$ at C before $R_{23}^-(\eta)$ arrives at the corresponding sonic stem. This characteristic curve Γ_- continues to pass through R_{23}^- and ends at E, and goes straight again until it is tangent to the sonic circle C_3 at G. By the discussion of

the last section, we kown that $\widehat{AP}$ and $\widehat{CE}$ are circular arcs. $\overline{AC}$ is tangent to $\widehat{AP}$ and $\widehat{CE}$ at A and C respectively, and $\overline{EG}$ is tangent to $\overline{CE}$ at E. The equivalent is true for Γ_+ from P. We illustrate these in Figure 3.1.

This case has two subcases depending on whether $\overline{EG}$ and $\overline{HF}$ are tangent to C_3 or not before they intersect each other. For simplicity, we just consider the case for $p_2 = p_4$. Then the solution is axially symmetric $\xi = \eta$. So the former occurs if and only if $0 < \dfrac{\eta_G}{\xi_G} \le 1$ or *vice versa* for the latter. This is because $\overline{EG}$ is perpendicular to the radius of C_3 through G. After a routine calculation, we arrive at

$$\frac{\eta_G}{\xi_G} = \frac{x(x-\sqrt{2x-1}) - (2-x)(x-1)^2}{(x-1)\sqrt{(2-x)[2x(x-\sqrt{2x-1}) - (2-)(x-1)^2]}}, \tag{3.4}$$

where $x = \dfrac{p_1}{p_3}$. It can be shown that there is a unique $x_0 (\doteq 1.84494)$ such that $\frac{\eta_G}{\xi_G} > 1$ if and only if $2 > x > x_0$. Thus we obtain

Theorem 3.1 *The characteristic curves Γ_- and Γ_+ from P are tangent to the sonic circle C_3 before they interact each other if and only if $2 > x > x_0 (\doteq 1.884494)$.*

The rarefaction waves R_{12}^+ and R_{41}^- interact at P to penetrate each other. The interaction domain is bounded by the characteristics Γ_- and Γ_+ from P (and a part of C_3 for the first subcase). So, we need to consider the Goursat problem for the system (2.1) with Γ_- and Γ_+ as the Cauchy support. The following theorem shows that this problem has a unique continuous supersonic rarefactive solution in a neighborhood of P.

Theorem 3.2 *The Goursat problem for (2.1) with $\widehat{PA}$ and $\widehat{PB}$ as the Cauchy support has a unique smooth supersonic solution in a neighborhood of P.*

To prove this theorem, we consider this problem in the polar coordinates (r, θ) with $r = \sqrt{\xi^2 + \eta^2}$ and $\tan\theta = \dfrac{\eta}{\xi}$. Let

$$\begin{pmatrix} U \\ V \end{pmatrix} = \begin{pmatrix} \cos\theta & \sin\theta \\ -\sin\theta & \cos\theta \end{pmatrix} \begin{pmatrix} u \\ v \end{pmatrix}.$$

Then (2.1) can be written as

$$AW_r + BW_\theta + c = 0 \tag{3.5}$$

where

$$A = \begin{pmatrix} -r & 0 & 1 \\ 0 & -r & 0 \\ p & 0 & -r \end{pmatrix}, \quad B = \begin{pmatrix} 0 & 0 & 0 \\ 0 & 0 & \dfrac{1}{r} \\ 0 & -\dfrac{p}{r} & 0 \end{pmatrix},$$

and

$$c = \left(0, 0, \frac{pU}{r}\right)^T, \quad w = (U, V, p)^T.$$

Here and in the following the superscript T represents the transposition of vectors. The eigenvalues of (3.5) are

$$\mu_0 = 0, \qquad \mu_\pm = \pm\frac{1}{r\sqrt{m-1}},$$

where $m = \dfrac{r^2}{p}$ is the square of Mach number. Then the characteristic curves are defined by

$$\frac{d\theta}{dr} = \mu_i, \quad i = 0, \pm,$$

and the left characteristic vectors l^0 and $l^\pm$ associated with μ_0 and $\mu^\pm$, respectively, are

$$(1, 0, 0), \qquad (-1, \pm\sqrt{m-1}, -\frac{r}{p}).$$

Thus, we can write (3.4) as the standard form,

$$\begin{cases} (-r, 0, 1)(\dfrac{\partial}{\partial r} + \mu_0 \dfrac{\partial}{\partial \theta}) \begin{pmatrix} U \\ V \\ p \end{pmatrix} = 0, \\ (0, -r, \pm\sqrt{m-1})(\dfrac{\partial}{\partial r} + \mu_\pm \dfrac{\partial}{\partial \theta}) \begin{pmatrix} U \\ V \\ p \end{pmatrix} = \mu_\pm r U \triangleq b_\pm. \end{cases} \tag{3.6}$$

Introduce the notation

$$\begin{gathered} \frac{d}{d_i r} = \frac{\partial}{\partial r} + \mu_i \frac{\partial}{\partial \theta}, \quad i = 0, \pm, \\ l_0 = (-r, 0, 1), \quad l_\pm = (0, -r, \pm\sqrt{m-1}), \end{gathered} \tag{3.7}$$

where $\dfrac{d}{d_i r}$ represents the directional derivative along the i^{th} characteristic curve. So we express (3.6) as

$$\begin{cases} l_0 \cdot \dfrac{dw}{d_0 r} = 0, \\ l_\pm \cdot \dfrac{dw}{d_\pm r} = b_\pm. \end{cases} \tag{3.8}$$

Now we begin to consider the interaction of R_{12}^+ and R_{14}^- in a neighborhood of P. In the polar coordinate system–the (r, θ)-plane, the circular arcs $\widehat{PA}$ and $\widehat{PB}$ can be expressed as

$$\begin{gathered} \widehat{PA} : r = 2\cos\theta, \quad (\pi/4 \le \theta \le \theta_A), \\ \widehat{PB} : r = 2\sin\theta, \quad (\theta_B \le \theta \le \pi/4), \end{gathered} \tag{3.9}$$

where p_1 is assumed to be 1, θ_A and θ_B are the polar angles of A and B. Thus, the Cauchy data of this Goursat problem are

$$\begin{aligned} W|_{\widehat{PA}} &= (2\cos 2\theta \cos\theta, -2\cos 2\theta \sin\theta, 4\cos^4\theta)^T \triangleq w^-, \\ W|_{\widehat{PB}} &= (-2\cos 2\theta \sin\theta, -2\cos 2\theta \cos\theta, 4\sin^4\theta)^T \triangleq w^+. \end{aligned} \tag{3.10}$$

To guarantee that the Goursat problem has a unique smooth solution, we can further check the following compatibility conditions are satisfied.

(1) $w^-(P) = w^+(P)$. This is obvious from (3.9).

(2)

$$\begin{aligned} l_- \cdot \frac{dw^-}{d_- r}\Big|_{\widehat{PA}} &= \mu_- r U|_{\widehat{PA}}, \\ l_+ \cdot \frac{dw^+}{d_+ r}\Big|_{\widehat{PB}} &= \mu_+ r U|_{\widehat{PB}}. \end{aligned}$$

These show that the Cauchy data on $\widehat{PA}$ and $\widehat{PB}$ are compatible with the equations (3.6).

(3)

$$\frac{1}{\mu_+ - \mu_0} l_0 \cdot \frac{dw^+}{d_+ r} \mid_P = \frac{1}{\mu_- - \mu_0} l_0 \cdot \frac{dw^-}{d_- r} \mid_P \tag{3.11}$$

This equation shows that at P, the Cauchy data on $\widehat{PB}$ is compatible with that on $\widehat{PA}$. As a matter of fact, from (3.7), we have

$$\begin{aligned} l_0 \cdot \frac{dw}{d_- r} &= l_0 \cdot (\frac{dw}{d_- r} - \frac{dw}{d_0 r}) = l_0 \cdot (\mu_- - \mu_0) \frac{\partial w}{\partial \theta}, \\ l_0 \cdot \frac{dw}{d_+ r} &= l_0 \cdot (\frac{dw}{d_+ r} - \frac{dw}{d_0 r}) = l_0 \cdot (\mu_+ - \mu_0) \frac{\partial w}{\partial \theta}. \end{aligned} \tag{3.12}$$

Noticing that $P = (\sqrt{2}, \pi/4)$ in the (r, θ)-plane and then substituting (3.6) into these equations, we can check that (3.11) holds.

By now, Theorem 3.2 follows by the theorems in the paper [WW]. □

The numerical solution in Figure 3.2 illustrates that there is a subsonic region inside the interaction domain of four exterior rarefaction waves and the supersonic rarefactive solution extends continuously towards the sonic curve. The paper [Z] showed that a positive H^1_{loc} solution exists provided that the sonic curve belongs to $C^{2,\alpha}$. An open problem is how we can extend the local rarefactive solution in a neighborhood of P to the sonic curve and determine the regularity of the sonic curve. An other open problem is whether the pressure vanishes in a subset of the interaction domain. The initial data for Figure 3.2 is $p_1 = 0.525$, $p_2 = 0.2252$, $p_3 = 0.0155$, $\lambda^x = \lambda^y = 0.2$ with time steps $n = 540$.

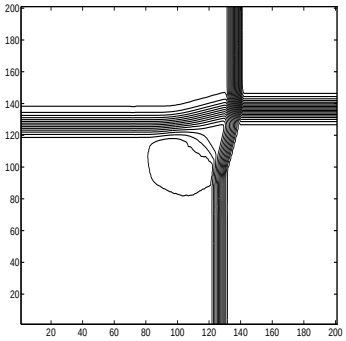

Configuration A

Pressure contour curves

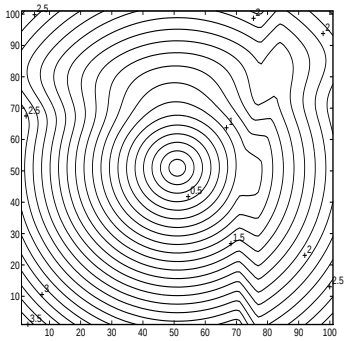

Configuration A

Pseudo-Mach number contour curves

Figure 3.2.

Configuration B $R^+_{12} R^-_{23} R^+_{34} R^-_{41}$. For this case, we have the system (B)

$$\begin{aligned} R^+_{12}: &\quad u_1 - u_2 = \Phi_{12}, &\quad v_1 - v_2 = 0, &\quad p_1 > p_2, \\ R^-_{23}: &\quad v_2 - v_3 = -\Phi_{23}, &\quad u_2 - u_3 = 0, &\quad p_2 < p_3, \\ R^+_{34}: &\quad u_3 - u_4 = -\Phi_{34}, &\quad v_3 - v_4 = 0, &\quad p_3 > p_4, \\ R^-_{14}: &\quad v_4 - v_1 = \Phi_{41}, &\quad u_1 - u_4 = 0, &\quad p_4 < p_1, \end{aligned} \tag{3.13}$$

from which, we obtain $p_1 = p_3 > p_2 = p_4$. It follows that $u_1 = u_4 > u_2 = u_3$, $v_1 = v_2 > v_3 = v_4$ and $u_1 - u_2 = v_1 - v_4$. Hence, for any fixed $p_1 > p_2$, u_1, v_1, we can get p_3 and p_4, u_i, v_i $(i = 2, 3, 4)$ from the first column and the second column of (3.13). This solution is symmetric with respect to $\xi - \eta = 0$ and $\xi + \eta = 0$.

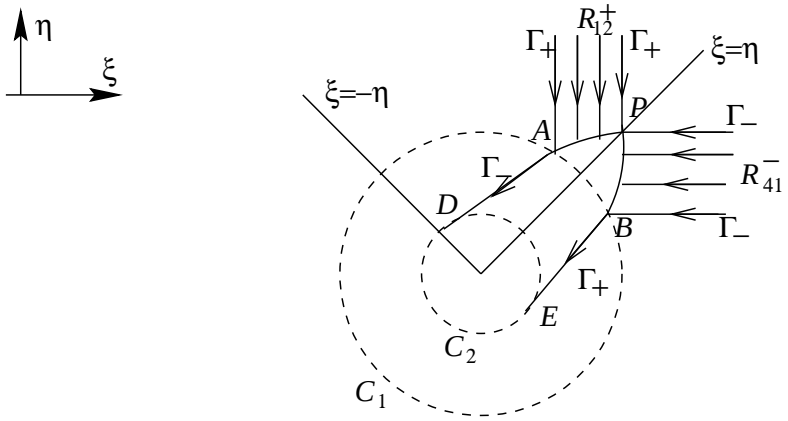

Figure 3.3

As shown in Figure 3.3, the two forward rarefaction waves R_{12}^+ and R_{41}^- coming from infinity interact at P. Then Γ_- (Γ_+) from P penetrates R_{12}^+ (R_{41}^-) firstly to enter into the constant state (p_2, u_2, v_2) ((p_4, u_4, v_4)) and are tangent to the sonic circle C_2 at $C(E)$. Symmetrically, $R_{23}^-(\eta)$ and $R_{34}^+(\xi)$ interact from Q. Γ_- (Γ_+) penetrates R_{34}^+ (R_{23}^-) to enter into (p_4, u_4, v_4) ((p_2, u_2, v_2)) and are tangent to C_2 at F (G).

Since the symmetric axes $\xi = \eta$ and $\xi = -\eta$ are just slip lines, which form compressive corners, the numerical solution shows that there are two symmetric shock waves separating the subsonic domain from the supersonic domains. With the same arguments, we can prove that the solution in a neighborhood of P (Q) is rarefactive. The problem is to solve the mixed-type equation (2.2) with the Cauchy data on Γ_- and Γ_+. The initial data for Figure 3.4 are $p_1 = 4.2$, $p_2 = 1.4$, $u_1 = 2$, $v_1 = 0.2677$, $\lambda^x = \lambda^y = 0.1$ with the time steps $n = 620$.

3.2 The interaction of four shocks. There are two kinds of configurations of solutions.

Configuration C $S_{12}^- S_{23}^+ S_{34}^- S_{14}^+$. For this case, the four constant states satisfy the system (C)

$$\begin{array}{lllll} S_{12}^-: & u_1 - u_2 = -\Psi_{12}, & v_1 = v_2, & p_1 > p_2, \\ S_{23}^+: & v_2 - v_3 = \Psi_{23}, & u_2 = u_3, & p_2 < p_3, \\ S_{34}^-: & u_3 - u_4 = \Psi_{34}, & v_3 = v_4, & p_3 > p_4, \\ S_{41}^+: & v_4 - v_1 = -\Psi_{41}, & u_2 = u_3, & p_4 < p_1. \end{array} \tag{3.14}$$

Similar to Configuration B, we can prove that $p_1 = p_3 > p_2 = p_4$. This results in

$$u_1 = u_4 < u_2 = u_3, \quad v_1 = v_2 < v_3 = v_4, \quad u_1 - u_2 = v_1 - v_4.$$

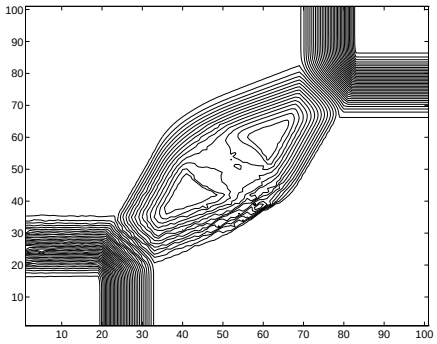

Configuration B

Pressure contour curves

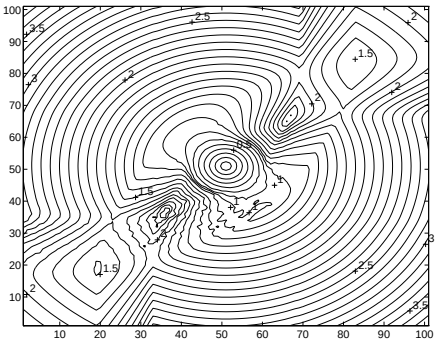

Configuration B

Pseudo-Mach number contour curves

Figure 3.4.

Therefore, the solution is symmetric to $\xi = \eta$ and $\xi = -\eta$. For any fixed $p_2 < p_1$, u_1, v_1, we can get u_i, v_i $(i = 2, 3, 4)$ from the first column and the second column of (3.14).

Let us analyze how the four shocks from infinity interact to match together. Obviously, if S_{12}^- and S_{23}^+ meet at the point $P = (\xi_0, \eta_0)$ before they reach the sonic circles C_1 and C_2, the collision of these two shocks results in the formation of two reflection shocks S_{15}^+ and S_{35}^-, which separate the constant states from the state (p_5, u_5, v_5), as shown in Figure 3.5. From (2.8), we have

$$\begin{aligned} u_5 - u_1 &= \frac{\xi_0 \bar{p}_{15} + \eta_0 \sqrt{\bar{p}_{15}(\xi_0^2 + \eta_0^2 - \bar{p}_{15})}}{\bar{p}_{15}(\xi_0^2 + \eta_0^2)}(p_5 - p_1), \\ u_5 - u_3 &= \frac{\xi_0 \bar{p}_{35} - \eta_0 \sqrt{\bar{p}_{35}(\xi_0^2 + \eta_0^2 - \bar{p}_{35})}}{\bar{p}_{35}(\xi_0^2 + \eta_0^2)}(p_5 - p_3), \end{aligned} \tag{3.15}$$

where $\bar{p}_{ij} = \dfrac{p_i + p_j}{2}$. Eliminating u_5 in (3.15) and noting that $p_1 = p_3$ and $\xi_0 = -\eta_0 = -\sqrt{\bar{p}_{12}}$, we get

$$u_3 - u_1 = \frac{2\eta_0 \sqrt{\bar{p}_{15}(\xi_0^2 + \eta_0^2 - \bar{p}_{15})}}{\bar{p}_{15}(\xi_0^2 + \eta_0^2)}(p_5 - p_1),$$

which is equivalent to

$$\sqrt{p_1 + p_2}(u_3 - u_1)x = 2\sqrt{2}\sqrt{x(p_1 + p_2 - x)}(x - p_1), \tag{3.16}$$

where $x = \bar{p}_{15}$. We get by solving (3.16) that

$$x_\pm = \frac{5p_1 + p_2 - \sqrt{-7p_1^2 + 10p_1p_2 + p_2^2}}{4}.$$

Therefore,

$$p_5 = \frac{3p_1 + p_2 - \sqrt{-7p_1^2 + 10p_1p_2 + p_2^2}}{2}.$$

It follows that p_5 is real if and only if $p_2/p_1 \geq 4\sqrt{2} - 5$. Obviously, if $p_2/p_1 \geq 4\sqrt{2} - 5$,

$$\xi_0^2 + \eta_0^2 - \frac{p_5 + p_1}{2} = \frac{1}{4}[3p_2 - p_1 + \sqrt{-7p_1^2 + 10p_1p_2 + p_2^2}] > 0.$$

Since

$$\xi_0^2 + \eta_0^2 - p_5 = \frac{1}{2}[p_2 - p_1 + \sqrt{-7p_2^2 + 10p_1p_2 + p_2^2}],$$

we see that $\xi_0^2+\eta_0^2-p_5>0$ if and only if $p_2/p_1>\dfrac{2}{3}$. Besides, it can be proved that

$$p_5-p_1=\frac{1}{2}[p_1+p_2-\sqrt{-7p_1^2+10p_1p_2+p_2^2}]>0,$$

if $p_2/p_1\geq 4\sqrt{2}-5$. Based on the above discussion, we obtain the following theorem.

Theorem 3.3 *S_{12}^- and S_{23}^+ interact at the point P if and only if*

$$1>p_2/p_1\geq 4\sqrt{2}-5.$$

The state (u_5,v_5,p_5) at the point P is supersonic if $1>p_2/p_1>2/3$; it is sonic if $p_2/p_1=2/3$; and it is subsonic if $2/3>p_2/p_1\geq 4\sqrt{2}-5$.

In view of symmetry, the symmetric axis $\xi=-\eta$ can be regarded as a rigid wall. Therefore, S_{15}^+ should be a regular reflection shock of S_{12}^-. We restate Theorem 3.4 as follows.

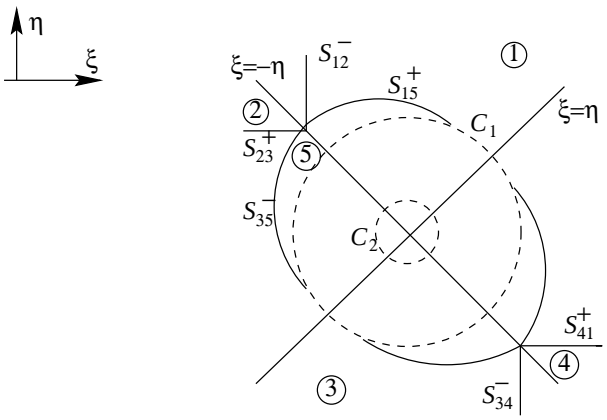

Figure 3.5

Theorem 3.3′ *For the shock S_{12}^-, the regular reflection shock occurs if and only if $1>p_2/p_1\geq 4\sqrt{2}-5$. The wave back of S_{15}^+ is supersonic if $1>p_2/p_1\geq 2/3$; sonic if $p_2/p_1=2/3$; and subsonic if $2/3>p_2/p_1\geq 4\sqrt{2}-5$.*

Thus, we can consider this configuration by two subcases according to the critical value $4\sqrt{2}-5$.

Subcase C_1 $1>p_2/p_1>4\sqrt{2}-5$. S_{12}^- and S_{23}^+ meet at P to form regular reflection shocks with the state (p_5,u_5,v_5) in between. If $1>p_2/p_1>2/3$, the state (p_5,u_5,v_5) is supersonic and S_{15}^+ is tangent to the R-H circles C_{15} at P. If $2/3>p_2/p_1>4\sqrt{2}-5$, (p_5,u_5,v_5) is subsonic or sonic, so S_{15}^+ separates (p_1,u_1,v_1) from the subsonic domain, goes straight until it reaches C_5, then bends towards C_5 clockwise, and becomes weaker and weaker. Finally, it ends at the intersection point of $\xi=\eta$ and C_{1*}, where p_* is the state on the wave back. The equivalent is true for S_{34}^- and S_{41}^+. We illustrate this subcase in Figure 3.6. The problem is to solve a free boundary value problem for (2.2) with the boundary consisting of reflection shocks and the parts of sonic circle for the former, or the reflection shocks for the latter. In the system of polar coordinates, the boundary conditions can be considered as follows. Letting $r=r(\theta)$ be a smooth discontinuity, we write (2.7)

and (2.8) in the form,

$$\begin{cases} \dfrac{dr}{d\theta} = -r\dfrac{[v]}{[u]} = \dfrac{\pm r\sqrt{r^2-p}}{\sqrt{\overline{p}}}, \\ [p] = r[u], \\ [p]^2 = \overline{p}([u]^2 + [v]^2). \end{cases}$$

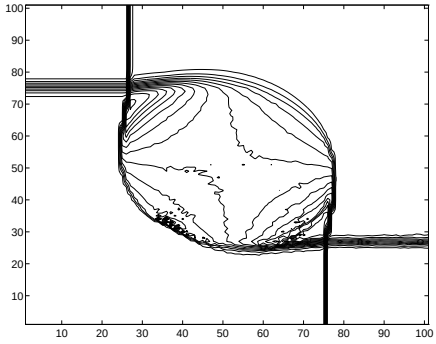

Configuration C_1

Pressure contour curves

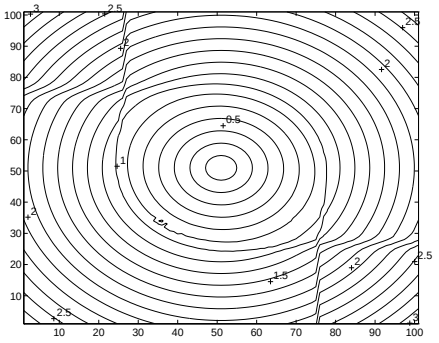

Configuration C_1

Pseudo-Mach number contour curves

Figure 3.6.

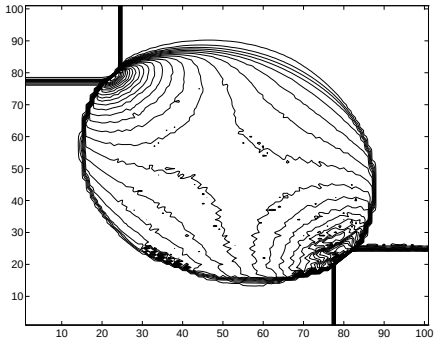

Configuration C_2

Pressure contour curves

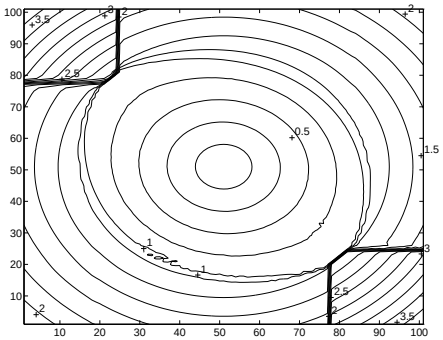

Configuration C_2

Pseudo-Mach number contour curves

Figure 3.7.

Then by some calculations, one can obtain that on $r = r(\theta)$ there holds

$$A(r, p, \overline{p})p_r + B(r, p, \overline{p})p_\theta = 0,$$

where

$$A = -\left(\frac{r^2-p}{p} + \frac{r^2-\overline{p}}{\overline{p}} - \frac{r^2(p-\overline{p})}{2\overline{p}^2}r^2\frac{dr}{d\theta}\right), \quad B = -\frac{2}{r^2}\left(\frac{dr}{d\theta}\right)^3 + \frac{r^2(p-\overline{p})}{2\overline{p}^2}.$$

Therefore, this problem is the free boundary problem for (2.2) with the directional derivative as the boundary value, which is something like the third Dirichlet boundary-value problem but is more difficult. It still remains open. We take the initial data for the numerical solution as $p_1 = 1.5$, $p_2 = 1.2$, $u_1 = -0.1291$, $v_1 = -0.1291$, $\lambda^x = \lambda^y = 0.1$ with time steps $n = 840$.

Subcase C_2 $p_2/p_1 < 4\sqrt{2} - 5$**.** For this subcase, the Mach reflection shock will occur. There is a triple configuration of shocks on S_{12}^-. The Mach stem reaches the rigid wall vertically, and the reflection shock separates (p_1, u_1, v_1) from the subsonic domain. The initial data for the numerical solution (see Configuration C_2) is $p_1 = 2.5$, $p_2 = 0.8$, $u_1 = 0$, $v_1 = 0$, $\lambda^x = \lambda^y = 0.05$ with the time steps $n = 1100$.

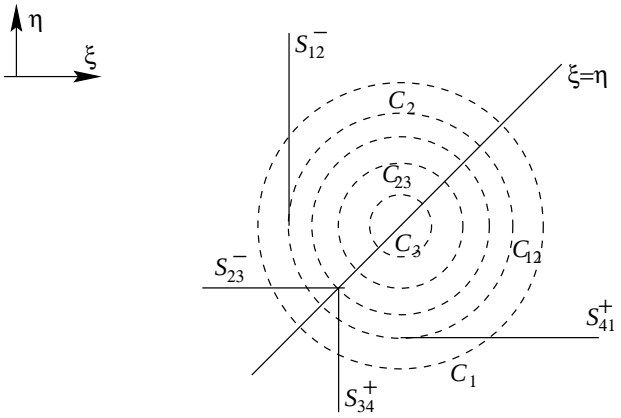

Figure 3.8

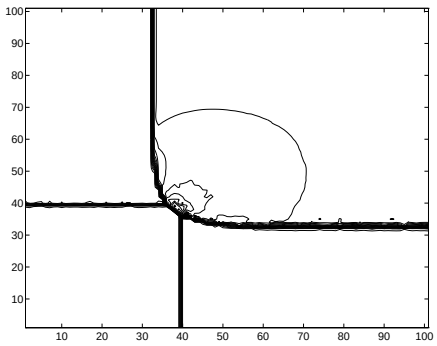

Configuration D

Pressure contour curves

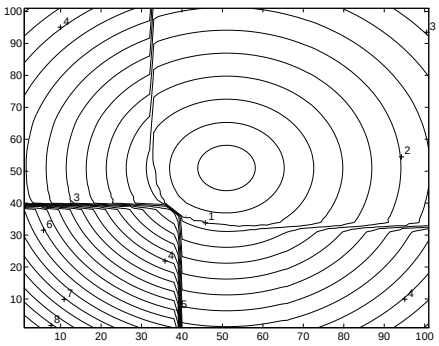

Configuration D

Pseudo-Mach number contour curves

Figure 3.9.

Configuration D $S_{12}^- S_{23}^- S_{34}^+ S_{14}^+$. For this case, we have the system (D)

$$\begin{array}{lllll} S_{12}^-: & u_1 - u_2 = -\Psi_{12}, & v_1 - v_2 = 0, & p_1 > p_2, \\ S_{23}^-: & v_2 - v_3 = -\Psi_{23}, & u_2 - u_3 = 0, & p_2 > p_3, \\ S_{34}^+: & u_4 - u_3 = -\Psi_{34}, & v_4 - v_3 = 0, & p_4 > p_3, \\ S_{14}^+: & v_1 - v_4 = -\Psi_{14}, & u_1 - u_4 = 0, & p_1 > p_4. \end{array} \tag{3.17}$$

Based on this system, we can verify that

$$p_2 = p_4, \quad (\frac{p_1}{p_2} + 1)(\frac{p_3}{p_2} + 1) = 4. \tag{3.18}$$

Therefore, $u_1 = u_4 < u_2 = u_3$, $v_1 = v_2 < v_3 = v_4$, $u_1 - u_2 = v_1 - v_4$. The solution is symmetric to $\xi = \eta$. For any fixed $p_2 < p_1$, u_1, v_1, we can obtain p_2 and p_4 from (3.18), u_i, v_i from the first and the second columns of (3.17).

Just as in Configuration C, $\xi = \eta$ can be viewed as a rigid wall. S_{23}^- meets $\xi = \eta$ before it reaches the sonic circle C_2. If $1 > p_3/p_2 > 4\sqrt{2} - 5$, then a regular reflection shock occurs. Otherwise, a Mach reflection shock appears. The reflection shock bends clockwise. S_{12}^- begins to bend counterclockwise with decreasing wave strength after it meets the sonic circle C_1. This shock matches the reflection shock on its R-H circle, where the minimum of the pressure is taken. The initial data for the numerical solution is $p_2 = 1.2$, $p_1 = 2.5$, $\lambda^x = \lambda^y = 0.05$ with time steps $n = 1100$.

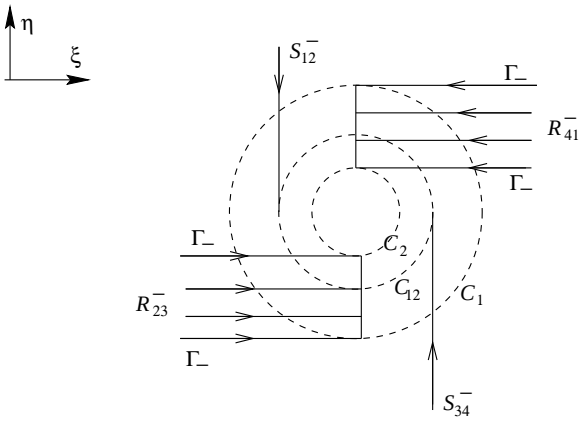

Figure 3.10

3.3 The interaction of two rarefaction waves and two shock waves Configuration E $S_{12}^- R_{23}^- S_{34}^- R_{14}^-$. The four constant states satisfy the system (E)

$$\begin{array}{lllll} S_{12}^-: & u_1 - u_2 = -\Psi_{12}, & v_1 - v_2 = 0, & p_1 > p_2, \\ R_{23}^-: & v_2 - v_3 = -\Phi_{23}, & u_2 - u_3 = 0, & p_2 < p_3, \\ S_{34}^-: & u_3 - u_4 = \Psi_{34}, & v_3 - v_4 = 0, & p_3 > p_4, \\ R_{41}^-: & v_4 - v_1 = \Phi_{41}, & u_4 - u_1 = 0, & p_4 < p_1. \end{array} \tag{3.19}$$

From this system, we obtain $p_1 = p_3 > p_2 = p_4$. So, $u_1 = u_4 < u_2 = u_3$, $v_1 = v_2 > v_3 = v_4$, $u_1 - u_2 = v_4 - v_1$. For any fixed $p_2 < p_1$, u_1, v_1, we can obtain p_3, p_4, and u_i, v_i $(i = 2, 3, 4)$ from the first and the second column from (3.19).

Since the solution is rotationally symmetric with the rotation angle $\alpha = \pi/2$, it suffices to consider R_{41}^- and S_{34}^-. S_{34}^- first meets the sonic circle C_3 and then bends inward to separate (p_4, u_4, v_4) from the subsonic domain with decreasing strength. This shock matches the weak shock resulting from R_{41}^- at its R-H circle C_{4*}, where p_* is the pressure on the wave back. The numerical results show that R_{41}^- extends to interact with S_{12}^-. There is a subsonic domain, being bounded by the shocks. The initial data we choose is: $p_1 = 2.525$, $p_2 = 1.4$, $u_1 = 0$, $v = 0.8116$, $\lambda^x = \lambda^y = 0.1$ with time steps $n = 480$.

3.4 The interaction of two rarefaction waves and two slip lines. We divide this into two cases, Configurations F and G. The initial data distribution satisfies $p_2 = p_3 = p_4$ and $u_1 = u_3 = u_4 > u_2$ and $v_1 = v_2 = v_3 > v_4$. For any fixed p_2, p_1, u_1, v_1, we can easily find u_i, v_i $(i = 2, 3, 4)$ from (2.10) and (2.12). The solution is symmetric to $\xi = \eta$.

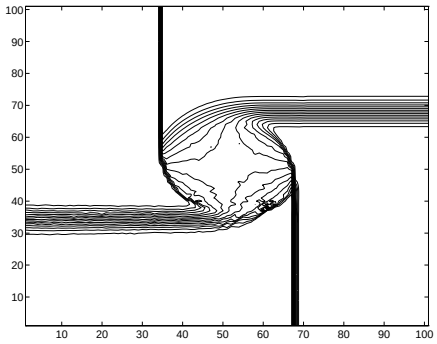

Configuration E

Pressure contour curves

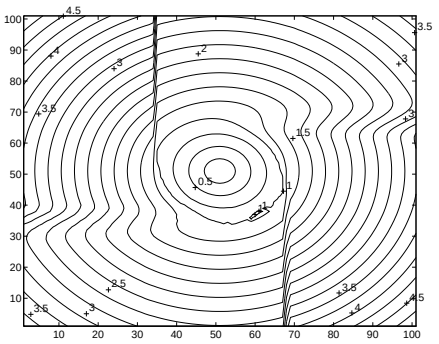

Configuration E

Pseudo-Mach number contour curves

Figure 3.11.

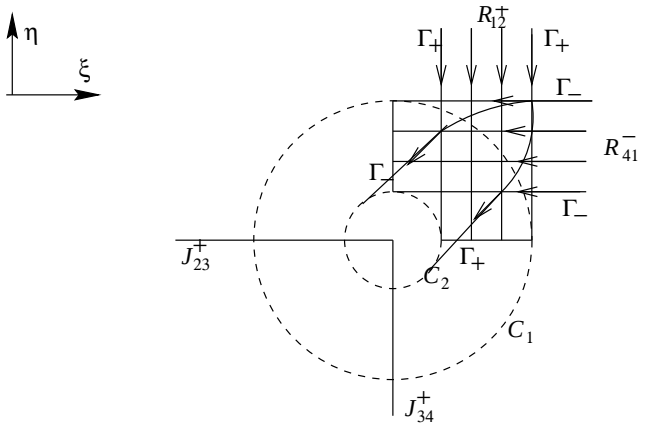

Figure 3.12

Configuration F $R_{12}^+ J_{23}^+ J_{34}^- R_{14}^-$. The four constant states satisfy the system (F)

$$\begin{array}{lllll} R_{12}^+: & u_1 - u_2 = \Phi_{12}, & v_1 - v_2 = 0, & p_1 > p_2, \\ J_{23}^+: & u_2 < u_3, & v_2 = v_3, & p_2 = p_3, \\ J_{34}^-: & u_3 = u_4, & v_3 > v_4, & p_3 = p_4, \\ R_{14}^-: & v_4 - v_1 = \Phi_{41}, & u_4 - u_1 = 0, & p_4 < p_1. \end{array} \tag{3.20}$$

So, $p_1 > p_2 = p_3 = p_4$. R_{12}^+ and R_{41}^- meet at P and interact with each other. Γ_- (Γ_+) from P penetrates R_{12}^+ (R_{41}^-) and are finally tangent to C_2. J_{23}^+ and J_{34}^- first reach C_3 and then enter into the subsonic domain. Therefore the interaction region is bounded by Γ_- and Γ_+ and the part of C_3. In view of Theorem 3.2, there exists a unique a rarefactive smooth solution in the neighborhood of P. R_{12}^+ and R_{41}^- penetrate each other. It seems from the numerical solutions that the part of the solution in the subsonic domain is compressive. We choose the initial data as $p_1 = 2.525$, $p_2 = 1.4$, $u_1 = 0$, $v_1 = -0.8116$, $\lambda^x = \lambda^y = 0.2$ with time steps $n = 400$.

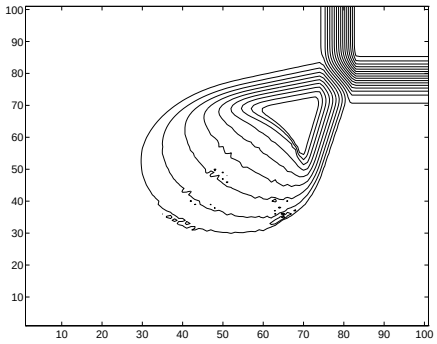

Configuration F

Pressure contour curves

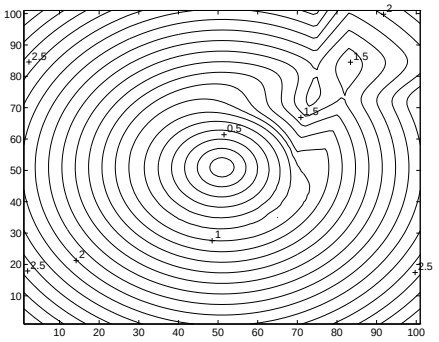

Configuration F

Pseudo-Mach number contour curves

Figure 3.13.

Configuration G $R_{12}^- J_{23}^+ J_{34}^- R_{14}^+$. The four constant states satisfy (G)

$$\begin{array}{lllll} R_{12}^-: & u_1 - u_2 = -\Phi_{12}, & v_1 - v_2 = 0, & p_1 < p_2, \\ J_{23}^+: & u_2 < u_3, & v_2 = v_3, & p_2 = p_3, \\ J_{34}^-: & u_3 = u_4, & v_3 > v_4, & p_3 = p_4, \\ R_{14}^+: & v_4 - v_1 = -\Phi_{41}, & u_4 - u_1 = 0, & p_4 > p_1. \end{array} \tag{3.21}$$

So, $p_1 < p_2 = p_3 = p_4$. R_{12}^- and R_{41}^+ reach their singularities. On the upper-right part, there exists a weak shock separating (p_1, u_1, v_1) from the subsonic domain. We will discuss this configuration carefully in the next section. Here we take the initial data for the numerical solution as $p_1 = 2.525$, $p_2 = 3.4$, $u_1 = 0$, $v_1 = -0.5098$, $\lambda^x = \lambda^y = 0.1$ with time steps $n = 520$.

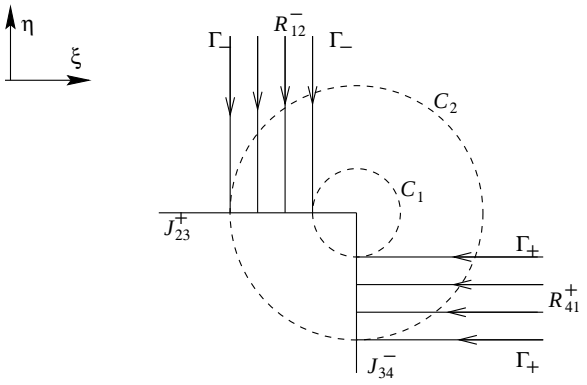

Figure 3.14

3.5 The interaction of two shocks and two slip lines. We also have two cases for this interaction, Configurations H and I. The four constant states satisfy $p_2 = p_3 = p_4$, $u_1 = u_3 = u_4 < u_2$ and $v_1 = v_2 = v_3 < v_4$. For any fixed p_2, p_1, u_1 and v_1, we can find u_i, v_i $(i = 2, 3, 4)$ from (2.11) and (2.12). The solution is symmetric to $\xi = \eta$.

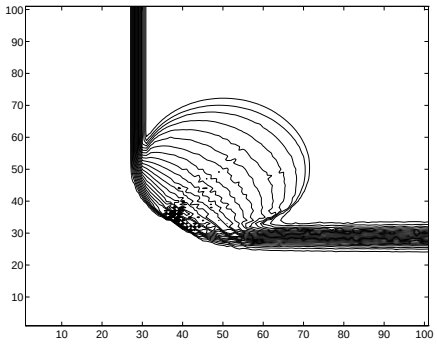

Configuration G

Pressure contour curves

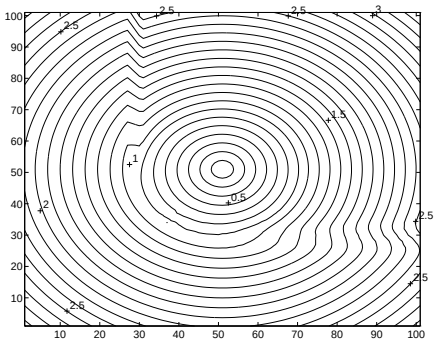

Configuration G

Pseudo-Mach number contour curves

Figure 3.15.

Configuration H $S_{12}^- J_{23}^- J_{34}^+ S_{14}^+$. For this case, we have the system (H)

$$\begin{array}{lllll} S_{12}^-: & u_1-u_2=-\Psi_{12}, & v_1-v_2=0, & p_1>p_2, \\ J_{23}^+: & u_2<u_3, & v_2=v_3, & p_2=p_3, \\ J_{34}^-: & u_3=u_4, & v_3>v_4, & p_3=p_4, \\ S_{41}^+: & v_1-v_4=-\Psi_{14}, & u_4-u_1=0, & p_4<p_1. \end{array} \tag{3.22}$$

So, $p_1 > p_2 = p_3 = p_4$. S_{12}^- and S_{41}^+ bends towards the upper right part after it reaches the sonic circle C_1. Then they becomes weaker and weaker until they match together at their R-H circle, as shown in Figure 3.16. These shocks bound a ball-like subsonic domain from below. The solution in the subsonic domain should be smooth and increasing along the radial direction. The initial data for the numerical solution is $p_1 = 2.525$, $p_2 = 1.4$, $u_1 = 0$, $v_1 = 0.8031$, $\lambda^x = \lambda^y = 0.1$ with the time steps $n = 540$.

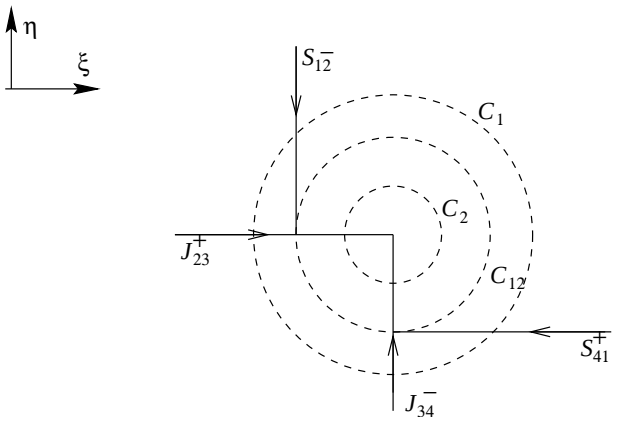

Figure 3.16

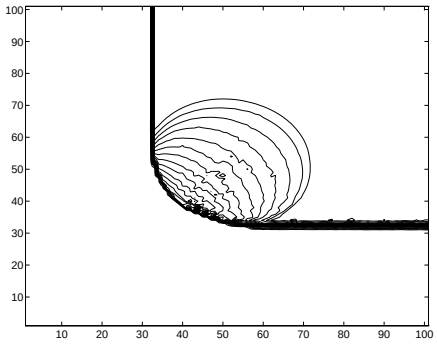

Configuration H

Pressure contour curves

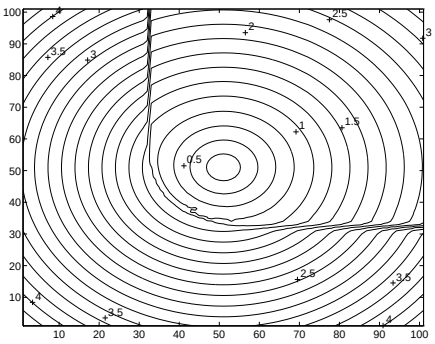

Configuration H

Pseudo-Mach number contour curves

Figure 3.17.

Configuration I $S_{12}^{+}J_{23}^{-}J_{34}^{+}S_{14}^{-}$. We have the system (I)

$$\begin{array}{lllll} S_{12}^{+}: & u_1-u_2=\Psi_{12}, & v_1-v_2=0, & p_1<p_2, \\ J_{23}^{+}: & u_2<u_3, & v_2=v_3, & p_2=p_3, \\ J_{34}^{-}: & u_3=u_4, & v_3>v_4, & p_3=p_4, \\ S_{41}^{-}: & v_1-v_4=\Psi_{41}, & u_4-u_1=0, & p_4>p_1, \end{array} \tag{3.23}$$

which gives $p_1 < p_2 = p_3 = p_4$. If $p_1/p_2 \geq 4\sqrt{2}-5$, S_{12}^{+} reaches $\xi=\eta$ and a regular reflection shock S_{2*} occurs with the state (p^*, u^*, v^*) on the wave back. The wave back of this shock at P is supersonic if $p_1/p_2 > 2/3$; sonic if $p_1/p_2 = 2/3$ and subsonic if $2/3 > p_1/p_2 > 4\sqrt{2}-5$. If $p_1/p_2 \leq 4\sqrt{2}-5$, the Mach reflection shock occurs in the same way as in Configuration D, see Figure 3.18. The reflection shock propagates with decreasing wave strength and finally vanishes at its R-H circle. Symmetrically, the equivalent is true for the reflection shock from S_{41}^{-}. These reflection shocks bound a subsonic domain, which is like a bubble. The initial data for the numerical solution is $p_1 = 2.525$, $p_2 = 4.4$, $u_1 = 0$, $v_1 = 1.0076$, $\lambda^x = \lambda^y = 0.1$ with time steps $n = 530$.

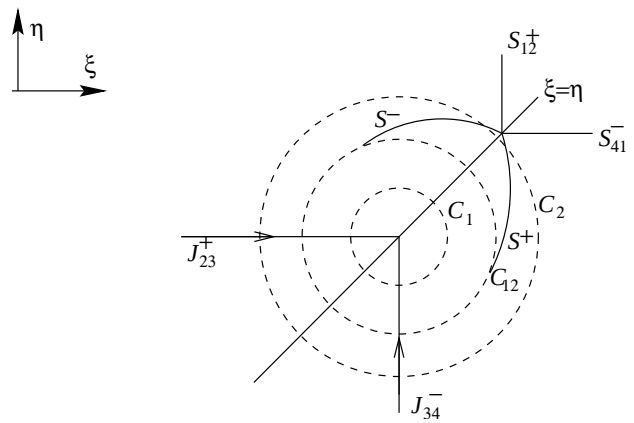

Figure 3.18

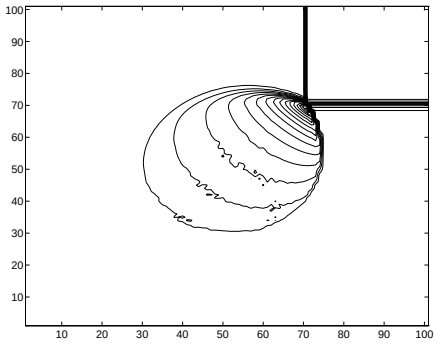

Configuration I

Pressure contour curves

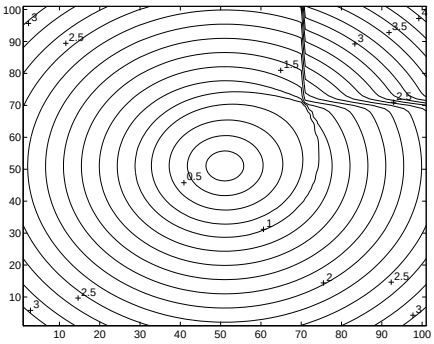

Configuration I

Pseudo-Mach number contour curves

Figure 3.19.

3.6 The interaction of a rarefaction wave, a shock and two slip lines. There are three cases for this interaction. The two involve two neighboring slip lines and the left involves two non-neighboring slip lines. Compared with the cases in Subsection 3.5, the solutions are no longer symmetric.

Configuration J $R_{12}^+ J_{23}^+ J_{34}^+ S_{41}^+$. The four constant states satisfy the system (J)

$$\begin{array}{lllll} R_{12}^+: & u_1 - u_2 = \Phi_{12}, & v_1 = v_2, & p_1 > p_2, \\ J_{23}^+: & u_2 < u_3, & v_2 = v_3, & p_2 = p_3, \\ J_{34}^+: & u_3 = u_4, & v_3 < v_4, & p_3 = p_4, \\ S_{41}^+: & v_4 - v_1 = -\Psi_{41}, & u_4 = u_1, & p_4 < p_1. \end{array} \tag{3.24}$$

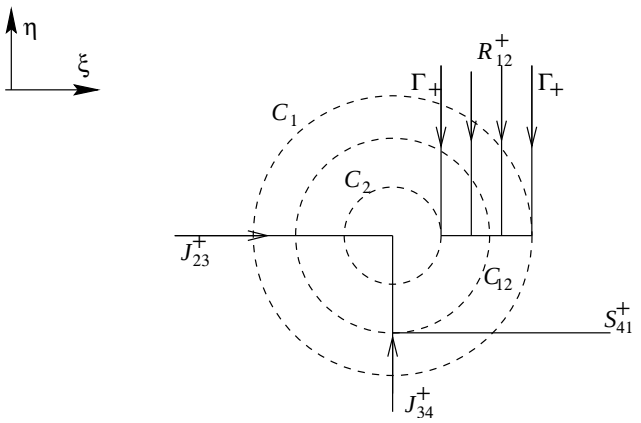

Figure 3.20

So, $p_1 > p_2 = p_3 = p_4$, $u_1 = u_3 = u_4 < u_1$, $v_1 = v_2 = v_3 < v_4$. The shock wave S_{41}^+ bends clockwise with decreasing wave strength after it reaches the sonic circle C_1. On the wave back of the rarefaction wave R_{12}^+ is a weak shock, which propagates and finally vanishes on its R-H circle. Thus, the shocks and the part of C_1 bound a subsonic domain. The initial data for the numerical solution is $p_1 = 2.5$, $p_2 = 1$, $u_1 = 0$, $v_1 = 0$, $\lambda^x = \lambda^y = 0.1$ with time steps $n = 620$.

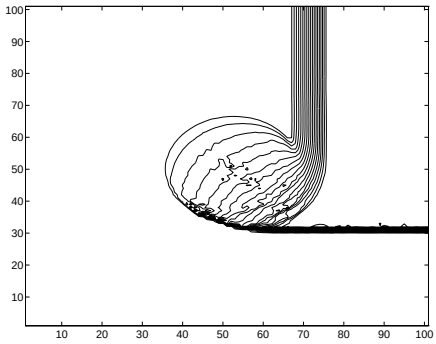

Configuration J

Pressure contour curves

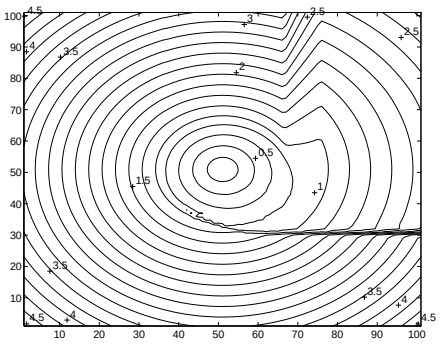

Configuration J

Pseudo-Mach number contour curves

Figure 3.21.

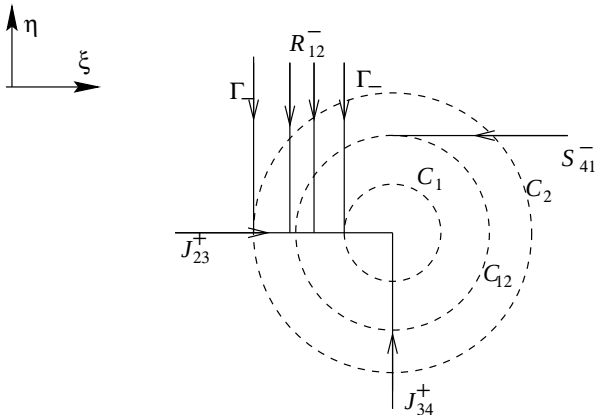

Figure 3.22

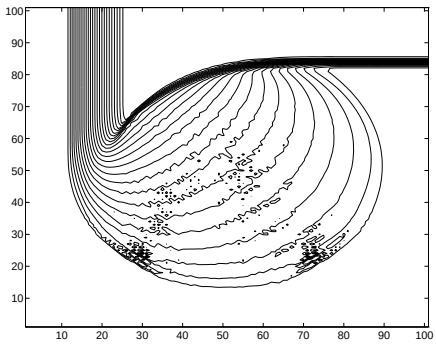

Configuration K

Pressure contour curves

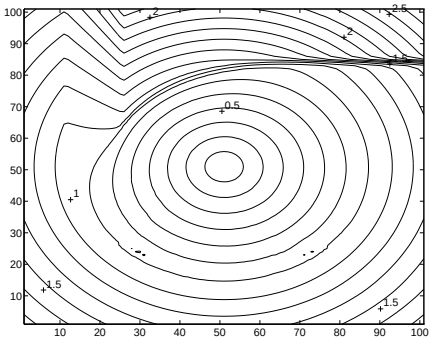

Configuration K

Pseudo-Mach number contour curves

Figure 3.23.

Configuration K $R_{12}^{-}J_{23}^{+}J_{34}^{+}S_{41}^{-}$. The four constant states satisfy the system (K)

$$\begin{array}{lllll} R_{12}^{-}: & u_1-u_2=-\Phi_{12}, & v_1=v_2, & p_1<p_2, \\ J_{23}^{+}: & u_2<u_3, & v_2=v_3, & p_2=p_3, \\ J_{34}^{+}: & u_3=u_4, & v_3<v_4, & p_3=p_4, \\ S_{41}^{-}: & v_4-v_1=\Psi_{41}, & u_4=u_1, & p_4>p_1, \end{array} \tag{3.25}$$

which results in $p_1 < p_2 = p_3 = p_4$, $u_1 = u_3 = u_4 < u_1$,$v_1 = v_2 = v_3 < v_4$. As in Configuration J, on the wave back of R_{12}^{-} is a shock. which matches the extension of S_{41}^{-} on the R-H circle. We take the initial data for the numerical result as $p_1 = 2.525$, $p_2 = 6.2$, $u_1 = 0$, $v_1 = 0$, $\lambda^x = \lambda^y = 0.1$ with the time steps $n = 640$.

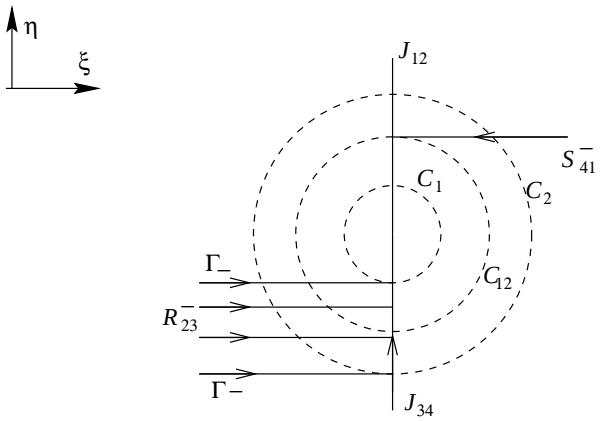

Figure 3.24

Configuration L $J_{12}R_{23}^{-}J_{34}S_{41}^{-}$. The four constant states satisfy the system (L):

$$\begin{array}{lllll} J_{12}: & u_1=u_2, & & p_1=p_2, \\ R_{23}^{-}: & v_2-v_3=-\Phi_{23}, & v_2=v_3, & p_2<p_3, \\ J_{34}: & u_3=u_4, & & p_3=p_4, \\ S_{41}^{-}: & v_4-v_1=\Psi_{41}, & u_2=u_3, & p_4>p_2. \end{array} \tag{3.26}$$

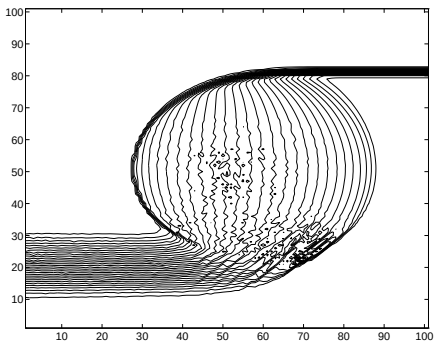

Configuration L

Pressure contour curves

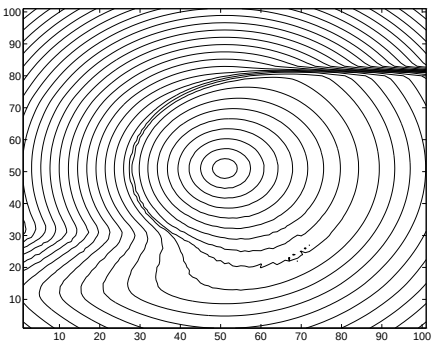

Configuration L

Pseudo-Mach number contour curves

Figure 3.25.

So, we have

$$p_1 = p_2 < p_3 = p_4, \quad u_1 = u_2 = u_3 = u_4.$$

The shock S_{41}^- stops at the R-H circle, where it matches the shock from R_{23}^-. The subsonic domain is bounded by the part of sonic circle from the lower-right and the shocks. The initial data we choose is $p_1 = 2.525$, $p_3 = 7.2$, $u_1 = 0$, $v_1 = 0$, $v_2 = -0.5$, $v_3 = -2.6885$, $v_4 = 2.1201$, $\lambda^x = \lambda^y = 0.1$ with time steps $n = 560$.

4. Discussions. Since the structures of solutions to two-dimensional Riemann problem for gas dynamics are conjectured in [ZZ], few analytic results are available to prove the complicated flowfield patterns. The present work just attempt to simplify the Euler system so that it is possible to establish analytic theories on the interaction of elementary waves in two dimensions. The results show that the slip lines have little influence on the structures of solutions so that the interaction of rarefaction waves and shocks can be studied thoroughly. The present paper also gives lots of flowfield patterns similar to those in [ZZ], but is much simpler. The criterion of transition from the regular reflection shock to the Mach reflection shock is presented and expected to be useful in the understanding of the oblique shock reflection.

In the self-similar plane, the pressure-gradient equations are of mixed-type. However, in many flowfield patterns presented here, the subsonic domain is bounded by shock waves and the parts of sonic circles, which proposes the free boundary-value problem for (2.1) with shocks and parts of sonic circles as the boundary. Owing to (2.8), we can solve this problem for (2.2) provided that the solution is smooth in the subsonic domain. So far, there is no general theory on the boundary-value problem for high-order partial different equations. The elegant second-order equation (2.2) may becomes a touchstone. By the observation on the numerical results, we find the maximum principle is taken in the subsonic domain.

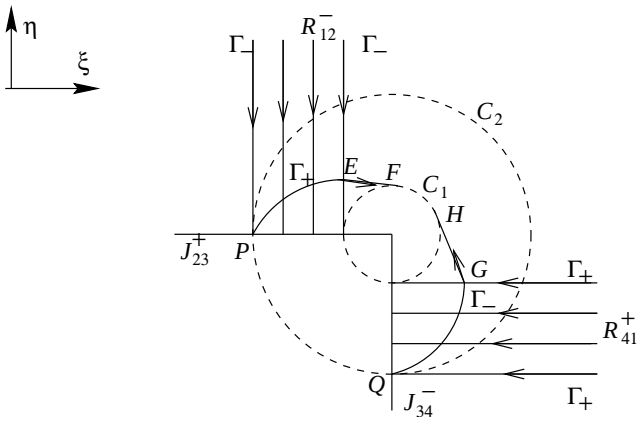

Figure 4.1

Our purpose to solve two dimensional Riemann problem is just to study how elementary waves interact. Oblique shock reflection is the most famous examples. In present paper, we classify elementary waves R, S, and J into two kinds, respectively. The numerical solutions shows that the interaction of rarefaction waves themselves, or rarefaction waves and other types of elementary waves may result in the occurrence of shocks, see Configurations A, B, F, E, G, J, K, L. These phenom-

ena are completely different from those in one dimension. We can further check that all these are compatible with the maximum principle aforementioned, which can be shown by taking Configuration G as an example, see Figure 4.1. Draw the characteristics Γ_+ and Γ^- from P and Q, respectively. They are tangent to the sonic circle C_1 at F and H. Then a quarter of C_2, the circular arc $\widehat{FH}$, Γ_+ and Γ_- bound a domain Ω, outside of which the solution is determined by the four constant states (u_i, v_i, p_i) $(i = 1, 2, 3, 4)$, and consists of four constant states, rarefaction waves R_{12}^- and R_{41}^+ and two slip lines J_{23}^+ and J_{34}^-. Assume the solution consists of rarefaction waves inside Ω. Then the solution takes its minimum at the origin because all slip lines point towards there, which contradicts the maximum principle.

References

[AH] R.K.Agarwal and D.W.Halt, A modified CUSP scheme in wave/particle split form for unstructed grid Euler flow, Frontiers of Computational Fluid Dynamics, *David A. Caughey and Mohamed M Hafez*, 1994:155-163.

[LC] Y. Li and Y. Cao, Second order "large particle" difference method, *Sciences in China,* in Chinese, **A.** 8. 1985.

[WW] R. H. Wang and Z. Q. Wu, On mixed initial boundary value problem for quasilinear hyperbolic system of partial differential equations in two independent variables, *J. Jilin University*, 2(1963), 459-502.

[WY] H. M. Wu and S. L. Yang, MmB- A new class of accurate high resolution schemes for conservation laws in two dimensions, *IMPACT of Computing in Sciences and Engineering,* 1(1989), 217-289.

[Z] Y. X. Zheng, Existence of solutions to the transonic pressure gradient equations of the compressible Euler equations in elliptic regions, to appear in Comm.in Partial Diff. Equat.

[ZZ] T. Zhang and Y. X. Zheng, Conjecture on the structure of solution of the Riemann problem for two-dimensional gas dynamics systems, *SIAM J. Math. Anal.* Vol. 21, No. 3, pp. 593-630, May, 1995.

Received for publication December 1997.

Email address
Peng Zhang: pzhanght.rol.cn.net
Jiequan Li: ljqamath6.amt.ac.cn
Tong Zhang: tzhangmath03.math.ac.cn